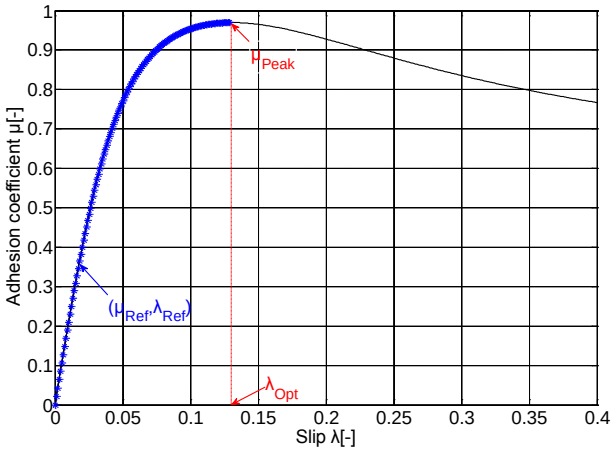

Figure 1 μ-λ curve

This paper is organized as follows: section 2 presents the adopted tyre model. Section 3 presents the structure of the adaptive friction control. The desired longitudinal slip ratio is calculated in section 4 and realized in section 5. At last, numerical simulation results are shown in section 6.

2 Tyre Model

The Magic Formula is applied in this paper, which is widely used to calculate steady-state tyre force and moment in vehicle dynamics studies. For a constant vertical load, the longitudinal friction coefficient is given by:

$$\mu_L = \mu(\lambda, B_L, C_L, D_L, E_L) = D_L \sin[C_L \arctan\{B_L\lambda - E_L(B_L\lambda - \arctan(B_L\lambda))\}] \quad (1)$$

where

μ_L longitudinal friction coefficient
λ wheel longitudinal slip
B_L stiffness factor
C_L shape factor
D_L peak value
E_L curvature factor

In fact, the working conditions of vehicle are uncertain, e.g., there are variations of road surface. So the key parameters of the Magic Formula B_L , C_L , D_L and E_L should be estimated on-line, which is one of the tasks for section 4.

3 Control Structure of Adaptive Type longitudinal Friction Control

The adaptive, or self-tuning tyre friction control, whose structure is diagrammatized in Figure 2, is a part of the main/servo loop control. The main loop is used to calculate the desired tyre friction and active wheel angles. And the servo loop is adopted to realize the optimal control inputs, i.e. tyre friction, which is exerted through brake and active wheel angle. In this paper, we only focuses on the longitudinal tyre friction control.

The control structure of the adaptive tyre friction control is as Figure 2. The desired tyre friction, which is calculated by the main loop, is the control objective, and the main purpose is to track this friction. Two steps are included in the adaptive tyre friction control:

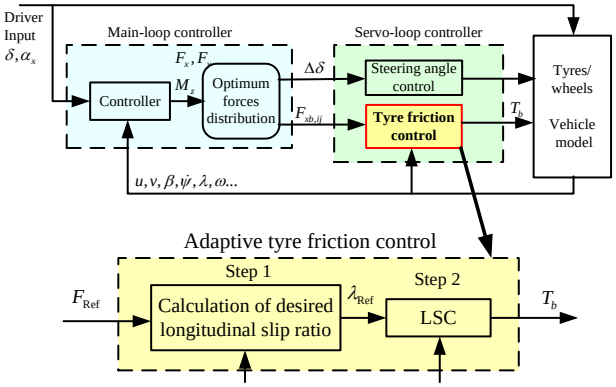

Figure 2 Schematic diagram of the main/serve loop structure and adaptive tyre friction control

Step 1: Calculation of the desired longitudinal slip ratio is the purpose of this step. Using constrained hybrid genetic algorithm (GA), the parameters of Magic Formula can be estimated on-line so that the tyre model is able to adapt to the variations of road surface. This means through this process, the controller is endowed to the ability of self-tuning to road variations. Then based on tyre model, the desired longitudinal slip ratio, which is corresponding to a given desired tyre friction, can be calculated via a numerical method.

Step 2: The Longitudinal Slip ratio Control (LSC) is employed to track the desired longitudinal slip ratio rapidly and precisely through exerting brake to the wheel. The nonsingular and fast terminal sliding mode (NFTSM) is applied to achieve good tracking ability.

4 Calculation of Desired Longitudinal Slip Ratio

Tyre friction estimation is a prerequisite for longitudinal friction control. For an electric vehicle with in-wheel motors, the brake and drive torque are measured by transducers mounted in motors. There has been an attempt to measure the brake torque of conventional vehicles by force transducer mounted on the brake caliper support[13]. In this paper, assume that the brake torque can be measured, and then the tyre friction can be estimated using the method discussed below.

A quarter-car model is shown in Figure 3. The dynamic equations of motion are as follows:

$$m\frac{du}{dt} = -F_{xb} \tag{1}$$

$$J\frac{d\omega}{dt} = r_b F_{xb} - T_b \tag{2}$$

$$F_Z = mg \tag{3}$$

where

m mass of the quarter-car
u vehicle horizontal speed
F_{xb} tyre friction
J wheel inertia
ω wheel angular speed
r_b wheel radius
T_b brake torque
F_Z vertical force
g acceleration of gravity

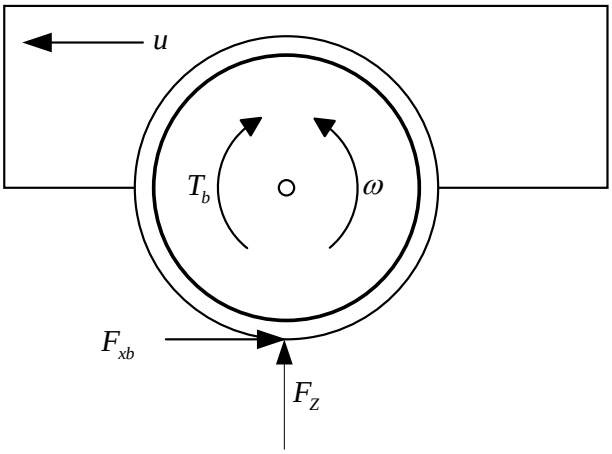

Figure 3 Quarter-car model

Then the tyre friction can be estimated by the following equation:

$$\hat{F}_{xb} = \frac{J}{r_b}\frac{d\omega}{dt} + \frac{T_b}{r_b} \tag{4}$$

The longitudinal slip ratio $\hat{\lambda}_{xb}$ with respect to $\hat{F}_{xb}$ is estimated by

$$\hat{\lambda}_{xb} = \frac{u - \omega r_b}{u} \tag{5}$$

The following equation is to describe the non-linear relationship of the tyre friction F_{xb} and the corresponding λ_{xb}

$$F_{xb} = F_Z \cdot \mu_{xb}(\lambda_{xb}) \tag{6}$$

where μ_{xb} is friction coefficient.

In order to minimize the error of the estimated values and the real values of B_L, C_L, D_L and E_L, this paper employs a performance index PI, i.e. the weighted sum of squares of the error between the estimated values and the real values of the tyre friction. Then the original parameter identification problem is converted to a constrained optimization problem and can be written as:

$$\min_x PI = \sum_{i=1}^{N} w_i \left[\hat{F}_{xb,i} - F_Z \mu\left(\hat{\lambda}_{xb,i}, x^T\right) \right]^2 \tag{7}$$

$$x = \left[B_L, C_L, D_L, E_L\right]^T \tag{9}$$

$$s.t.\ \ x_{\min} \le x \le x_{\max} \tag{10}$$

where w_i is the weighting factor, $x_{\min}$ and $x_{\max}$ are the lower and upper constrained bounds of B_L, C_L, D_L and E_L, respectively.

The scheme for minimizing PI is presented by using the constrained hybrid genetic algorithm, which optimizes PI using the Genetic Algorithm (GA) and the active-set Sequential Quadratic Programming (SQP) method. GA can reach the region near an optimum point quickly, but it takes many function evaluations to achieve convergence. This scheme is to run GA for a small number of generations to approach an optimum point. Then the solution from GA is used as an initial point for SQP approach for fast local search.

A GA can be an appropriate solution with respect to its powerful and global search technique based on the operation of natural genetics and the Darwinian 'survival of the fittest' theory with a randomly structured information exchange. Given an optimization problem, GA encodes the parameters concerned into finite bite binary strings, called a chromosome. And this is the first and important part of a GA process. A chromosome population subsequently forms, each represent a possible solution to the optimization problem. Evaluating the fitness of each chromosome according to the performance index is an important link between the GA and the practical system. Three basic operations, i.e., 'reproduction', 'crossover' and 'mutation', similar to genetic evolution, are then performed. 'Reproduction' is a process by which the strings with higher probabilities will breed large number of their copies in the new generation. The 'crossover' involves exchanging corresponding portions of binary strings at a random selected portioning position of two chromosomes, which are chosen from the parent strings. This process can combine better qualities among the preferred good strings and extend the genetic search space. 'Mutation' is a process by which the chance for the GA to reach the optimal point is reinforced through just an occasional alteration of a value at a randomly selected bit position, such as flipping the state of bit from 1 to 0, or vice versa. In the following, each of the strings is decoded to be its decimal values of corresponding actual parameters and sent to

objective function. At last, the string with the optimal value of performance index is found and decoded to obtain the parameters to be optimized for the reference tyre model.

Because of the features mentioned above, the GA is introduced to search the optimal values of B_L, C_L, D_L and E_L. And they are encoded into a binary string of fixed length as following.

$$\underbrace{\overbrace{B_L}^{S_1},\overbrace{C_L}^{S_2},\overbrace{D_L}^{S_3},\overbrace{E_L}^{S_4}}_{string}$$

Without losing generality and assuming that there are N1,N2, N3 and N4 bits for each value of B_L, C_L, D_L and E_L respectively, so the whole length of the string, i.e., the chromosome in GA optimized solution process, have N1+N2+N3+N4 bits. It leads to that, if

$$S_1 = \underbrace{10\cdots0100100}_{N1bits}$$

$$S_2 = \underbrace{00\cdots010101}_{N2bits}$$

… …

$$S_4 = \underbrace{10\cdots000101}_{N4bits}$$

and then the corresponding decimal values for B_L, C_L, D_L and E_L are given as

$$B_L = B_{L,\min} + \frac{d_{B_L i}}{2^{N1}-1}\left(B_{L,\max} - B_{L,\min}\right)$$

$$C_L = C_{L,\min} + \frac{d_{C_L i}}{2^{N2}-1}\left(C_{L,\max} - C_{L,\min}\right)$$

… …

$$E_L = E_{L,\min} + \frac{d_{E_L i}}{2^{N4}-1}\left(E_{L,\max} - E_{L,\min}\right)$$

where, $d_{B_x i}$, $d_{C_x i}$,…, $d_{E_x i}$ respectively represent the binary value for B_L, C_L, D_L and E_L.

Besides encoding the parameters and derivation of performance index, several important genetic parameters in the GA-based searching procedure, e.g. the generation number, population size, the crossover rate and the mutation rate, must be chosen. In the present study, the selection for these parameters based on previous experience is described in section 6.

Here the active set SQP approach is chosen as the hybrid function of GA, which is appropriate for small or large inequality constrained problems.

Firstly, the lower and upper bound constraints of equation (10) can be transformed into conventional inequality constraints as following

$$A_c x \geq b_c \tag{11}$$

$$A_c = \left[I, -I\right]^T, b_c = \left[x_{\min}, -x_{\max}\right]^T \tag{12}$$

where I is the 4×4 identity matrix.

Then the Lagrangian for the constrained problem (8) is defined as

$$L(x,\varphi) = PI(x) - \sum_{i\in\psi}\varphi_i\left(\alpha_i x - b_i\right) \tag{13}$$

where $i\in\psi$ are the inequality constraints. And in this section, the active set at any feasible x is

$$A_a(x) = \left\{i\in\psi \mid A_c x \geq b_c\right\} \tag{14}$$

For the inequality-constraints, the optimization problem (8) cannot be solved using Lagrangian methods directly. The active set SQP methods is extend the inequality-constrained problem to the equality-constrained problem [13-14]. Specifically, the approach selects a subset of constraints at each iteration $x^{(k)}$ to be the so-called working set $I^{(k)}$, and solves only equality-constrained subproblems, where the constraints in the working sets are imposed as equalities and all other constraints are ignored. The working set is updated at every iteration by rules based on Lagrange multiplier estimates. Suppose that at the iterate $\left(x^{(k)},\varphi^{(k)}\right)$, we define the quadratic programming:

$$\min\ q(p) = \nabla PI_k^T p + \frac{1}{2}p^T W_k p \tag{15a}$$

$$s.t.\quad A_k^T p + A_c\left(x_k\right) - b_c \geq 0 \tag{15b}$$

At working set $I^{(k)}$, we should solve the equality-constraints optimization problem as following:

$$\begin{aligned}&\min\ \nabla PI_k^T p + \frac{1}{2}p^T W_k p\\ &s.t.\quad a^i p + A_c^i\left(x^{(k)}\right) - b_c^i = 0, i\in I^{(k)}\end{aligned} \tag{16}$$

Define

$$\delta = p - p^{(k)}$$

We have

$$q\left(\delta + p^{(k)}\right) = \nabla PI_k^T\delta + \frac{1}{2}\delta^T W_k\delta + q\left(p^{(k)}\right) \tag{17}$$

where $q\left(p^{(k)}\right)$ is independent of q.

Since we can drop $q\left(p^{(k)}\right)$ from the objective without changing the solution of the problem, we can write the QP subproblem to be solved at the *kth* iteration as follows:

$$\min\ \nabla PI_k^T\delta + \frac{1}{2}\delta^T W_k\delta \tag{18a}$$

$$s.t.\quad a^i\delta = 0, i\in I^{(k)} \tag{18b}$$

Supposing for the moment that the optimal δ_k from (18a) is nonzero, we need to decide how far to move along this direction. If $p_k + \delta_k$ is feasible with respect to all the constraints, we set $p_{k+1} = p_k + \delta_k$. Otherwise, we set

$$p_{k+1} = p_k + \alpha_k\delta_k \tag{19}$$

To maximize the decrease in q, we want α_k to be as large as possible in [0, 1] subject to retaining feasibility, so we obtain the following definition

$$\alpha_k \overset{def}{=} \min\left(1, \min_{i\notin I^{(k)}, a^i\delta<0} \frac{b_{c,i} - a_{c,i}^T p_k}{a_{c,i}^T \delta_k}\right) \tag{20}$$

Any SQP method relies on a choice of W_k (an approximation of the Hessian of the Lagrangian) in the quadratic model. One way to approximate the Lagrangian Hessian would be to use a quasi-Newton approximation, such as the BFGS update formula with Hessian approximation B_k rather than W_k, we set

$$\begin{aligned} s_k &= x_{k+1} - x_k \\ y_k &= \nabla_x L(x_{k+1}, x_{k+1}) - \nabla_x L(x_k, x_k) \end{aligned} \tag{21}$$

$$B_{k+1} = B_k - \frac{B_k s_k s_k^T B_k}{s_k^T B_k s_k} + \frac{y_k y_k^T}{s_k^T y_k} \tag{22}$$

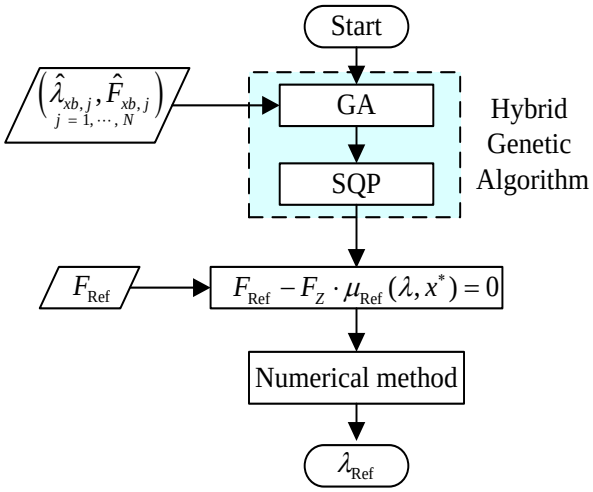

Figure 4 Flow chart for calculating desired wheel slip ratio

However, if $\nabla_{xx}^2 L$ is positive definite at the sequence of points x_k, the method will converge rapidly; If $\nabla_{xx}^2 L$ is not positive definite, then using the BFGS update may not work well.

To ensure that the update is always well-defined the damped BFGS updating for SQP was devised. Using this scheme, we define

$$r_k = \theta_k y_k - (1-\theta_k) B_k s_k \tag{23}$$

where the scalar θ_k is defined as

$$\theta_k = \begin{cases} 1, & \text{if } s_k^T y_k \geq 0.2 s_k^T B_k s_k \\ \dfrac{0.8 s_k^T B_k s_k}{s_k^T B_k s_k - s_k^T y_k}, & \text{if } s_k^T y_k < 0.2 s_k^T B_k s_k \end{cases} \tag{24}$$

Update B_k as follows

$$B_{k+1} = B_k - \frac{B_k s_k s_k^T B_k}{s_k^T B_k s_k} + \frac{r_k r_k^T}{s_k^T r_k} \tag{25}$$

It guarantees that B_{k+1} is positive definite.

The desired longitudinal slip ratio λ_{Ref}, which is corresponding to the desired tyre friction F_{Ref} (which is also the reference tyre friction) obtained from the main loop, can be calculated by using the numerical method of nonlinear equations as follows:

$$F_{\text{Ref}} - F_Z \cdot \mu_{\text{Ref}}^*(\lambda_{\text{Ref}}) = 0 \tag{26}$$

The flow chart of the calculation of desired longitudinal slip ratio is shown in Figure 4.

5 LSC Based on NFTSM

A non-singular fast terminal sliding mode (NFTSM) method, which has great tolerance to parameter uncertainties and external disturbances, is proposed for LSC[16]. It has such advantages that if the system state is far away from the equilibrium, the system runs on linear sliding mode; and if the system state is near equilibrium, the system runs on nonsingular terminal sliding mode. Consequently, compared with linear- hyper-plane-based sliding mode control, NFTSM offers superior properties, such as fast response and convergence in finite time. It speeds up the convergence rate when the system is far away from the equilibrium point in comparison with non-singular terminal sliding mode (NTSM). Furthermore, it can avoid the singularity in FTSM control systems. The design process is discussed in the following paragraphs.

Firstly, we define a time-varying sliding mode surface as following:

$$s = \dot{e} + \alpha e + \beta e^{\frac{p}{q}} \tag{27}$$

where $e \in R$; α, β are constant and $\alpha > 0$; p, q are the given positive odd integers and $p < q < 2p$. The error is defined as:

$$e = \lambda - \lambda_{\text{Ref}} \tag{28}$$

From equations(5), (6) and (28), the following equation can be obtained:

$$\dot{e} = \frac{\frac{-r_b^2 F_{xb}}{J} + (1-\lambda)\dot{u}}{u} + \frac{T_b r_b}{uJ} - \dot{\lambda}_{\text{Ref}} \tag{29}$$

Then, the FTSM control law can be obtained as follows:

$$T_b = \frac{u \cdot J}{r_b}\left[-\frac{\ddot{e}}{\alpha} - \frac{\beta \cdot p}{\alpha \cdot q} \cdot e^{\frac{p}{q}-1} \cdot \dot{e} - \frac{\frac{-r_b^2 F_{xb}}{J} + (1-\lambda)\dot{u}}{u} + \dot{\lambda}_{\text{Ref}}\right] \tag{30}$$

The sliding mode control process involves two phases: the reaching phase and the sliding phase. And the discontinuous control is usually employed in order to deliver a finite time reachability of the switching manifolds. But it is one of the major

contributors to the "chattering" behaviors well known existed in sliding mode control. Furthermore, the control law (30) has a singularity problem because of $p/q - 1 < 0$. Consequently, to avoid this phenomenon, a new "terminal attractor" is proposed to develop a chattering free NFTSM control without the singularity problem. It is shown as follows:

$$\dot{s} = (-\phi s - \gamma s^{\frac{m}{n}}) e^{\frac{p}{q}-1} \tag{31}$$

where $\phi \in R^+$; $\gamma \in R^+$; m and n are the given positive odd integers and $0 < m/n < 1$ .From equations (27), (28),(29) and (31), the NFTSM control law can be obtained as follows:

$$T_b = \frac{u \cdot J}{r_b}\left\{\frac{q}{\beta \cdot p}\left[-\ddot{e} \cdot e^{1-\frac{p}{q}} - \alpha \cdot \dot{e} \cdot e^{1-\frac{p}{q}} + (-\phi s - \gamma s^{\frac{m}{n}})\right]\right.$$
$$\left. - \frac{\frac{-r_b^2 F_{xb}}{J} + (1-\lambda)\dot{u}}{u} + \dot{\lambda}_{\text{Ref}}\right\} \tag{32}$$

From equation(32), the system is able to converge to equilibrium by following the sliding surface, without the singularity problem because of $0 < 1 - p/q$.

From equation $s = 0$, it can be obtained that:

$$e^{-\frac{p}{q}}\dot{e} + \alpha e^{1-\frac{p}{q}} = -\beta \tag{33}$$

Let $z = e^{1-\frac{p}{q}}$, the following equation can be obtained:

$$\frac{d}{dt}z + \frac{q-p}{q}\alpha z = -\frac{q-p}{q}\beta \tag{34}$$

when $e = 0$, $z = 0$, $t = t_{si}$. Solving the differential equation (18), tsi can be obtained as follows:

$$t_{si} = -\frac{q}{\alpha(q-p)} \ln \frac{\alpha x(0)^{\frac{q-p}{q}} + \beta}{\beta} \tag{35}$$

It can be derived that t_{si} is a finite value, i.e. the system states will reach the system equilibrium in finite time. That is to see if the control law in equation (32) is chosen, the system states will reach the sliding equilibrium according to the terminal attractor in equation (31) in finite time t_{si} .

6 Simulation Results and Analysis

In this section, simulations are carried out to verify the effectiveness of the proposed controllers. The identification performance is verified in the first place and then the tracking ability of LSC is tested and the superiority of the NFTSM is compared with NTSM. At last, the whole performance of the adaptive friction control is shown under μ-jump road surface.

Table 1. Parameters used in simulations

Notation	Value	Unit
m mass of quarter-car	382.5	kg
u vehicle velocity	120	km/h
g acceleration of gravity	9.8	m/s^2
J wheel inertia	12	$kg \cdot m^2$
r_b wheel radius	0.25	m
N_{data} number of sampling points	10	-
$B_{L,\min}$ lower bond of stiffness factor	8	-
$C_{L,\min}$ lower bond of shape factor	1	-
$D_{L,\min}$ lower bond of peak value	0.1	-
$E_{L,\min}$ lower bond of curvature factor	0.1	-
$B_{L,\max}$ upper bond of stiffness factor	18	-
$C_{L,\max}$ upper bond of shape factor	1.7	-
$D_{L,\max}$ upper bond of peak value	1.5	-
$E_{L,\max}$ upper bond of curvature factor	0.9	-
GA: initial population size	30	-
GA: max number of generation	100	-
GA: crossover rate	0.2	-
GA: mutation rate	0.8	-

Table 2 Parameters of different road surface

Road	BL	CL	DL	EL
Snow	17.430	1.4500	0.20	0.6500
Cobblestone, wet	14.027	1.4500	0.40	0.6000
Asphalt, wet	15.635	1.6000	0.80	0.4500
Cobblestone, dry	10.695	1.4000	0.85	0.6450
Concrete, dry	13.427	1.6402	0.97	0.5372
Asphalt, dry	13.427	1.5500	1.10	0.5327

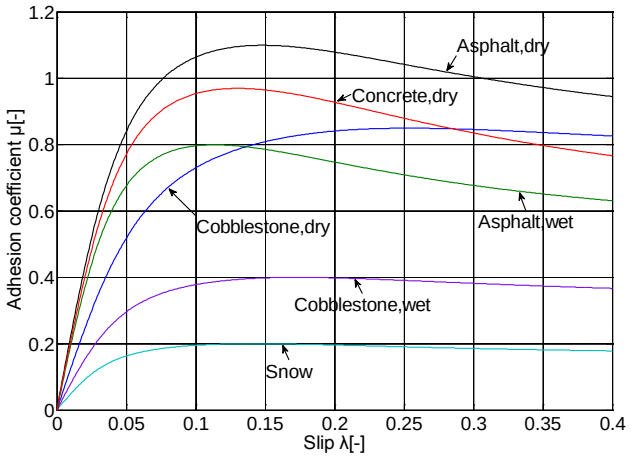

Figure 5. μ-λ curve of different road surface

The parameters used in the simulations are presented in Table 1.The empirical parameters of the Magic Formula for some common road surfaces

are presented in Table 2. According to these information, we can obtain the constrained range of B_L, C_L, D_L and E_L, respectively. The μ -λ curve of different road surface are shown in Figure 5.

a. Verification of parameters identification

In order to examine the effectiveness of the proposed identification scheme, simulations are carried out in many different cases, e.g. in the different range of sampling points $\hat{F}_{xb}$ and $\hat{\lambda}_{xb}$. The identification results are shown in Figures 6-14. Here the true value of μ is plotted using the true value of B_L, C_L, D_L and E_L, the identified value of μ is plotted using the identified value of B_L, C_L, D_L and E_L.

Given $\hat{\lambda}_{xb,j}\ (j=1,2,\cdots,N_{data})$ evenly distributed in the range $[0,0.01]$, as shown in Figure 6, the identified value of μ is satisfactory in the range $\lambda \in [0,0.08]$. The error of true and identified value of μ is less than 0.02, and the percentage error is no more than 2%, as shown in Figure 7 and Figure 10 respectively.

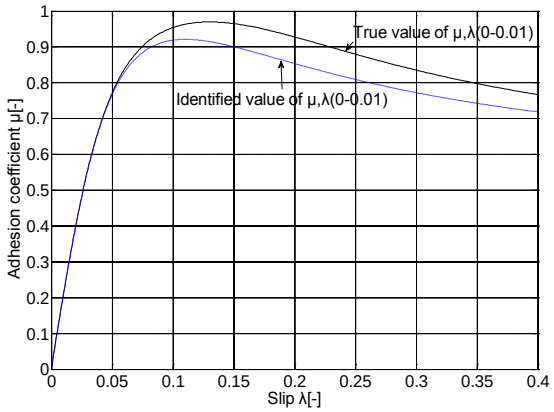

Figure 6. True and identified value of μ $(\lambda \in [0,0.01])$

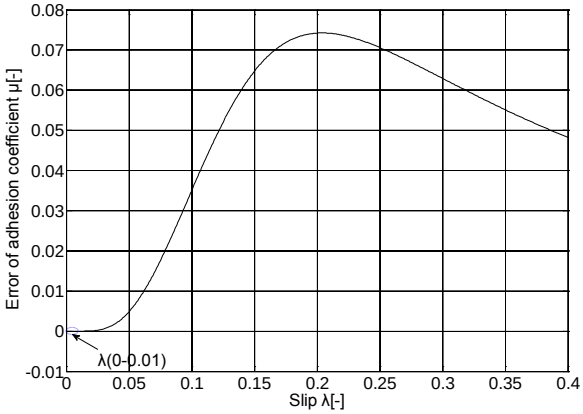

Figure 7. Error of true and identified value of μ $(\lambda \in [0,0.01])$

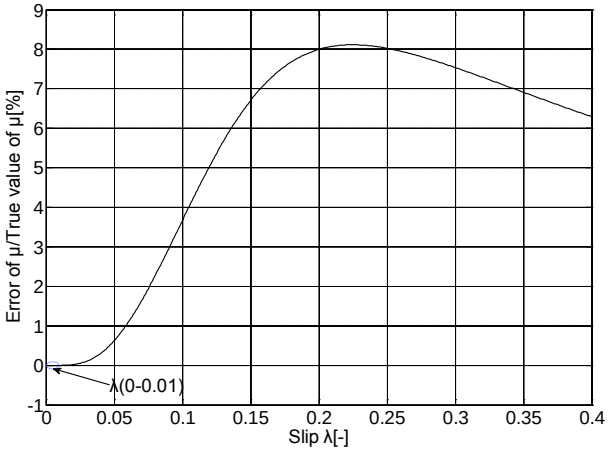

Figure 8. Percentage error of μ $(\lambda \in [0,0.01])$

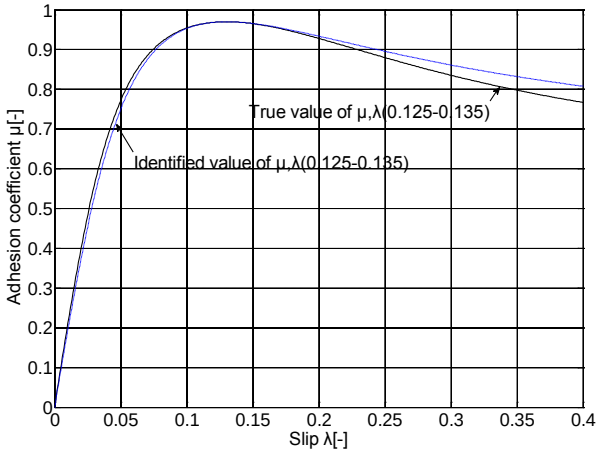

Figure 9. True and identified value of μ $(\lambda \in [0.125,0.135])$

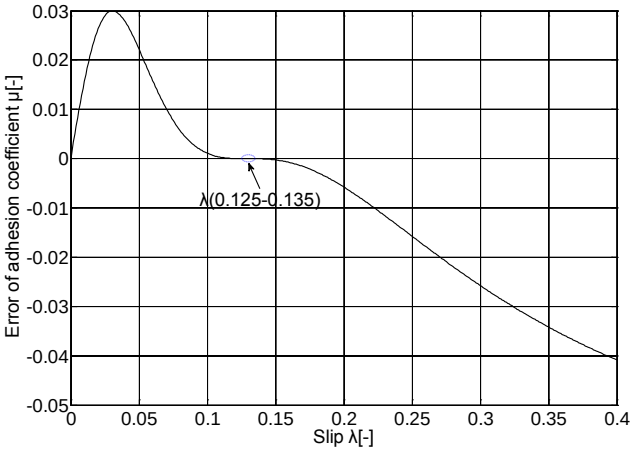

Figure 10. Error of true and identified value of μ $(\lambda \in [0.125,0.135])$

As can be seen in Figure 9, when we change the range of sampling points $\hat{\lambda}_{xb,j}\ (j=1,2,\cdots,N_{data})$ from $[0,0.01]$ to $[0.125,0.135]$, the identification result is significantly improved for these points containing more useful information of the non-linear characteristics of tire-road friction. As shown in

Figure 10 and Figure 11, in the range $\lambda \in [0.06, 0.25]$, the error of true and identified value of μ is less than 0.02, and the percentage error is no more than 2%. Furthermore, in the range $\lambda \in [0, 0.4]$, the maximum error is approximately equal to 0.03(Figure 10). The percentage error is largely less than 5%, indicated in Figure 10.

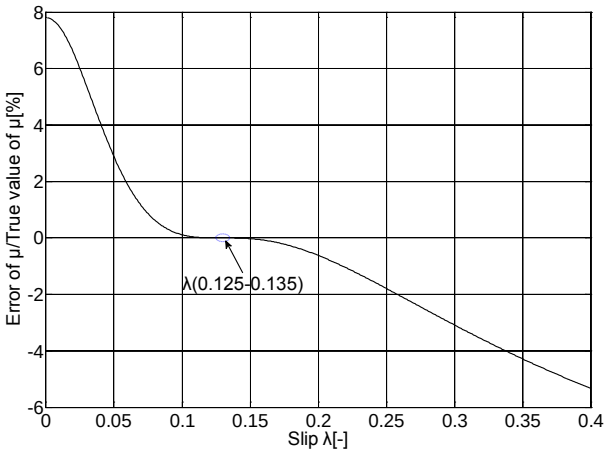

Figure 11. Percentage error of μ ($\lambda \in [0.125, 0.135]$)

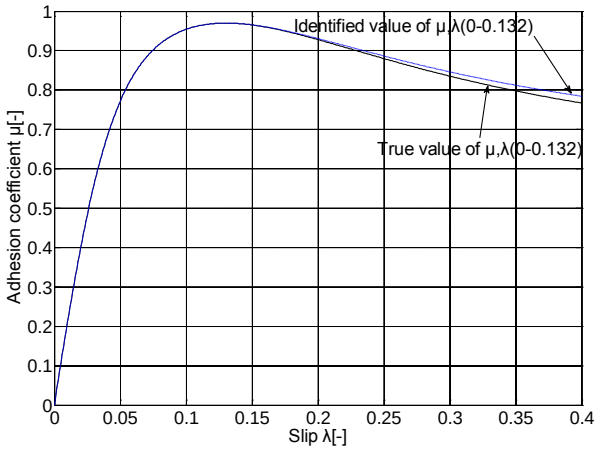

Figure 12. True and identified value of μ ($\lambda \in [0, 0.132]$)

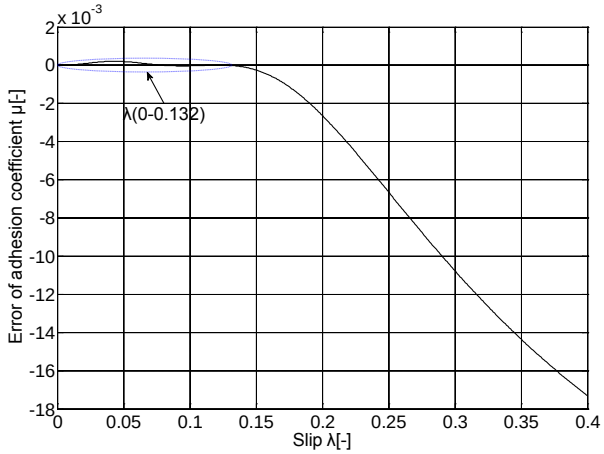

Figure 13. Error of true and identified value of μ ($\lambda \in [0, 0.132]$)

For further useful information, we expand the range of $\hat{\lambda}_{xb,j}$ ($j = 1, 2, \cdots, N_{data}$) to $[0, 0.132]$, Figure 12 shows the satisfactory performances more clearly. In the range $\lambda \in [0, 0.15]$ ($\lambda_{Opt} = 0.13$), the maximum error of true and identified value of μ is approximately equal to 2×10^{-4} (Figure 13). And the percentage error is no more than 0.03%, Figure 14.

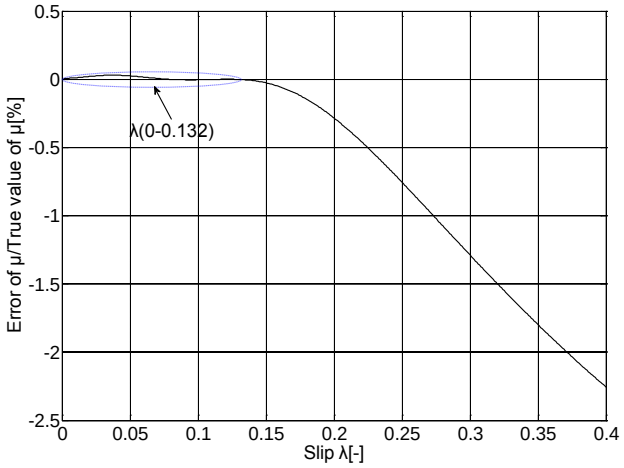

Figure 14. Percentage error of μ ($\lambda \in [0, 0.132]$)

As mentioned above, the more useful information of the sampling points $\hat{\lambda}_{xb}$ and the more accurate identification results of the B_L, C_L, D_L and E_L. It shows the more remarkable effect of the proposed method. However, in this paper, the values of B_L, C_L, D_L and E_L are identified on-line, the chosen points can only be located in the neighborhood of a given λ. Based on the above analysis, the identification results are satisfactory in these ranges, as shown in Figure 6-14.

b. Verification of LSC tracking ability

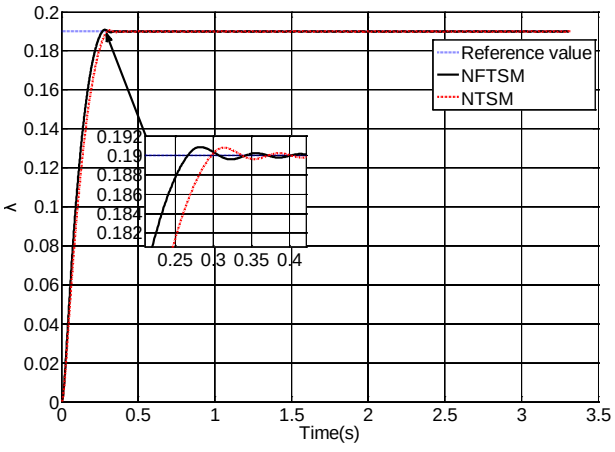

Figure 15 LSC tracking ability

To testify the effectiveness of the NFTSM, the reference value of $\lambda_{Ref} = 0.19$ is given to the LSC

controller to track. From Figure 15, it can be concluded that the NFTSM is in shorter response time than NTSM. Besides, the system is continuous, without appearance of a singular phenomenon.

c. Simulation results under μ-jump road surface

In the simulation of μ-jump road surface, the desired tyre friction $F_{\mathrm{Re}f}$ input is 2624N after 0.5s. At 1.5s, the vehicle drives from asphalt, wet road to asphalt, dry road. Simulation results are shown in Figure 16-19.

As is depicted in Figure 16-17 and Figure 19, with respect to tire friction, since NFTSM can use both the linear term $\dot{e}+\alpha e$ and the nonlinear fractional term $\beta e^{p/q}$ to obtain a corrective control force, the values of NFTSM tracks the reference value in faster response than that of NTSM after 0.5s and 1.5s. Consequently, the response of vehicle acceleration of NFTSM is also more sensitive than that of NTSM, as is shown in Figure 18. This proves the proposed control strategy to be effective in tracking desired tyre friction and in adaptation to the variation in road surface.

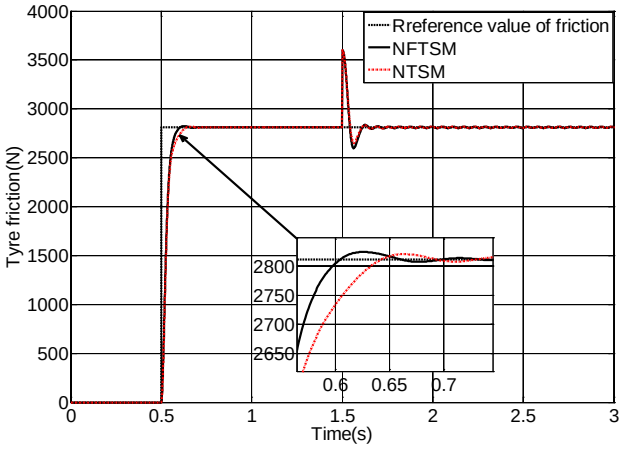

Figure 16 Tracking performance of tyre friction

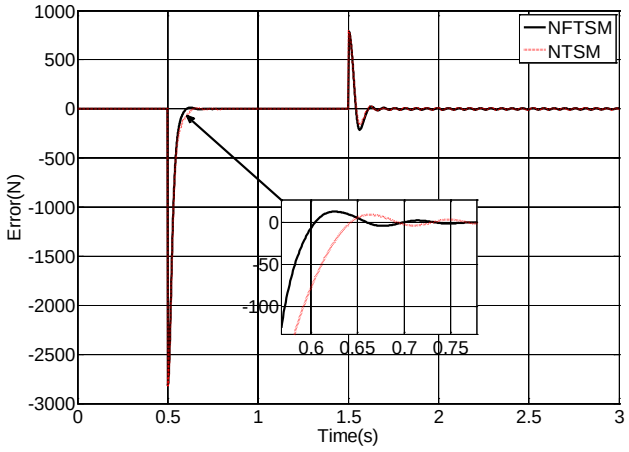

Figure 17 Tracking error of tyre friction

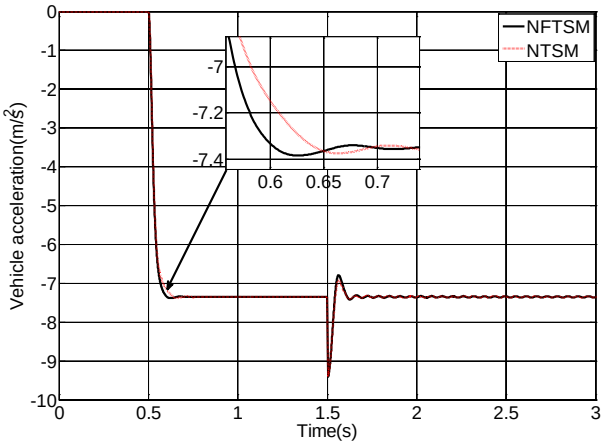

Figure 18 Vehicle acceleration

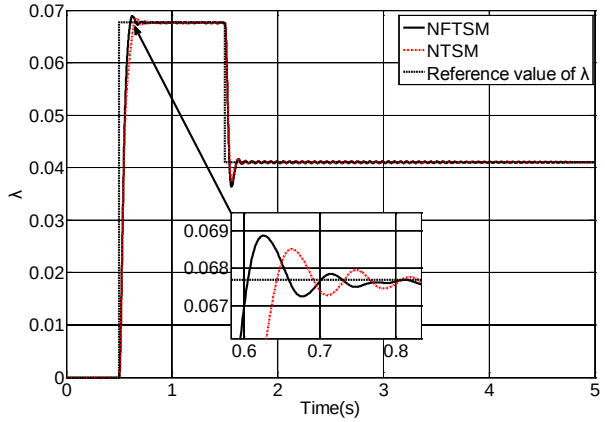

Figure 19 Tracking performance of slip ratio

In Figure 17, the tracking error of longitudinal tyre friction, while not as "perfect", is still very good and a smooth control law is now achieved.

7 Conclusion

Our main/servo loop control strategy is a representative of the vehicle integrated control, an active domain of research. This paper specifically focuses on a component of the servo loop to realize adaptive tyre friction control adaptive to the variation of road condition. A two-step solution is proposed: on-line identifying Magic Formula parameters using a hybrid GA method and correspondingly acquiring LSC objective using a numerical method, and dynamically implementing LSC using a nonsingular and fast terminal sliding mode (NFTSM) control method. In spite of a higher computation load compared with other control methods, a drastic optimization of the algorithms allows the controller provides a fast adaptation to the change in road surface condition and the simulation results shows that the tyre friction was tracked precisely and rapidly.

Ongoing researches endeavors on studying vehicle integrated control in a comprehensive way, consisting of, integrating the proposed adaptive

friction controller and the main loop controller and introducing robust control into the main loop to tackle parameter uncertainties.

ACKNOWLEDGEMENT – The authors would like to thank the Specialized Research Fund for the Doctoral Program of Higher Education of China under Grant No. 20100073110063 and the Science Fund of Key Laboratory of Vehicles Detection, Diagnosis & Maintenance technology for its great support.

References:

[1] Xiao, H., et al., Integrated control of active suspension system and electronic stability programme using hierarchical control strategy: theory and experiment. Vehicle System Dynamics, 2011. 49(1-2): p. 381-397.

[2] Gordon, T., M. Howell, and F. Brandao, Integrated control methodologies for road vehicles. Vehicle System Dynamics, 2003. 40(1-3): p. 157-190.

[3] F. Neri, "A Comparative Study of a Financial Agent Based Simulator Across Learning Scenarios", Agents and Data Mining Interaction, Lecture Notes in Computer Science 7103, Springer Berlin, 2012, pp. 86-97.

[4] Nagai, M., M. Shino, and F. Gao, Study on integrated control of active front steer angle and direct yaw moment. JSAE Review, 2002. 23(3): p. 309-315.

[5] J. H. Lee, W. S. Yoo.Non-singular slip (NSS) method for longitudinal tire force calculations in a sudden braking simulation,International Journal of Automotive Technology,February 2012, Volume 13, Number 2,pp. 215 - 222.

[6] Yu, F., D.F. Li, and D. Crolla. Integrated Vehicle Dynamics Control-state-of-the art review. in Vehicle Power and Propulsion Conference. 2008: IEEE.

[7] Yongchao Zhang, Guoguang Zhang, Fan Yu, Modeling and μ Synthesis Control of Vehicle Active Suspension with Motor Actuator, WSEAS Transactions on System, 2012, 11(5):173-186.

[8] Yao li, Jianwu Zhang, Xiqiang Guan, Estimation of Vehicle Parameters and Road Friction Using Steering Torque and Wheel Speeds, WSEAS Transactions on System, 2012,11(1):1-11.

[9] Huan-Jung Lin, Tain-Sou Tsay, Modeling Identification and Simulation of Bank to Turn Unmanned Aerial Vehicle, WSEAS Transactions on System, 2011,10(4):91-103.

[10] He, Z. and X. Ji, Nonlinear robust control of integrated vehicle dynamics. Vehicle System Dynamics, 2012. 50(2): p. 247-280.

[11] Hattori, Y., K. Koibuchi, and T. Yokoyama, Force and moment control with nonlinear optimum distribution for vehicle dynamics, in 6th International Symposium on Advanced Vehicle Control (AVEC'02). 2002: Hiroshima, Japan. p. Paper 024.

[12] Shen, X. and F. Yu, Study on vehicle chassis control integration based on a main-loop-inner-loop design approach. Proceedings of the Institution of Mechanical Engineers, Part D: Journal of Automobile Engineering, 2006. 220(11): p. 1491-1502.

[13] Li D., Yu F. A novel integrated vehicle chassis controller coordinating direct yaw moment control and active steering, SAE paper 2007-01-3642.

[14] Li, D., S. Du, and F. Yu, Integrated vehicle chassis control based on direct yaw moment, active steering and active stabiliser. Vehicle System Dynamics, 2008. 46(S1): p. 341-351.

[15] Jorge Nocedal, Stephen J.Wright. Numerical Optimization (Second Edition), Springer, 2006, pp: 467-540.

[16] Ishige, T., et al., Adaptive Slip Control using a Brake Torque Sensor, in 9th International Symposium on Advanced Vehicle Control (AVEC'08). 2008: Kobe, Japan